Molecular Wires

DOI: 10.1002/anie.201208481

Electrical Switching Behavior of a [60]Fullerene-Based Molecular Wire Encapsulated in a Syndiotactic Poly(methyl methacrylate) Helical Cavity**

Shengli Qi, Hiroki Iida, Lili Liu, Stephan Irle,* Wenping Hu, and Eiji Yashima**

As a class of unique nanocage molecules with a specific size, fullerenes have attracted considerable attention in the advanced materials sciences because of their potential applications in electronics[1] and optoelectronics.[2] The control and arrangement of these nanocages into ordered nanostructures is a great challenge, and has been extensively investigated in the last few decades.[3,4] Among them, the most attractive and impressive approach is the uniform one-dimensional (1D) alignment of fullerenes inside carbon nanotubes (CNTs), namely fullerene nanopeapods.[4] Theoretical calculations reveal that the fullerene nanopeapods have the potential to provide intriguing chemical and physical properties,[5] as frequently shown by experiments.[6] However, the encapsulation of fullerenes within CNTs remains difficult in terms of large-scale production and processability. We have recently developed a unique and versatile method to control the distinct 1D arrays of fullerenes in a commodity plastic, syndiotactic poly(methyl methacrylate) (st-PMMA), thus producing a peapod-like fullerene-based molecular wire.[7] The st-PMMA folds into a helical conformation and encapsulates the fullerenes, such as C_{60}, C_{70}, and C_{84}, within its helical cavity to form a peapod-like crystalline complex (Figure 1 A).[7a] In sharp contrast to other fullerene-containing polymer hybrids,[8] which often encounter considerable phase separation and aggregation, the st-PMMA/fullerene inclusion complex can be readily processed into homogeneous films by drop casting, spin coating, or Langmuir-Blodgett (LB) techniques.[7a] The fullerene molecules in the films are dispersed at the molecular level and are highly ordered into 1D peapod fullerene arrays, as illustrated in Figure 1 A.

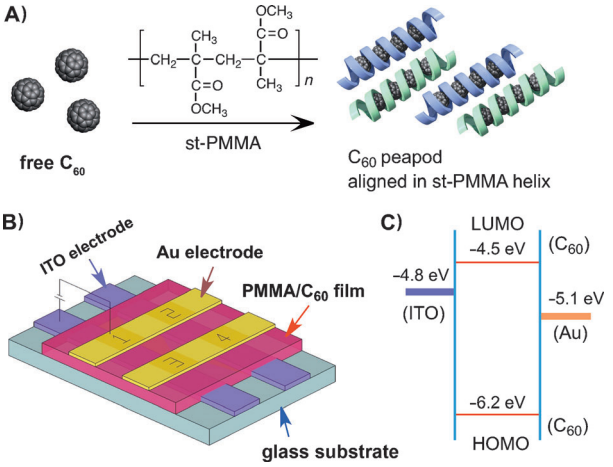

Figure 1. A) Illustration of C_{60}-based 1D molecular wire formation within the st-PMMA helical cavity. B) Diagram of the sandwiched memory device with the st-PMMA/C_{60} inclusion complex as the active layer. Bottom electrode: ITO (20 Ω sq^{-1}); top electrode: Au (ca. 20 nm thick). C) Energy level diagram for the sandwich device.

In the present study, we investigated the electrical characteristics of the st-PMMA/C_{60} inclusion complex, as C_{60} has been reported to possess a very strong electron affinity and can be reduced to anions with charges ranging from −1 to −6,[9] which indicates that C_{60} acts as an effective electron "nanotrap"[10] in electroactive processes. We expected that ordered C_{60} molecular wires in the st-PMMA matrix might help to realize unique electrical features. To this end, sandwich devices using the C_{60}-based molecular wire embedded in the cavity of helical st-PMMA[7] as the active layer were fabricated by spin coating a toluene solution of st-PMMA/C_{60} onto an indium tin oxide (ITO) electrode on a glass substrate, followed by thermal evaporation of a thin gold layer as the top electrode, as shown in Figure 1 B.

[*] Dr. S. Qi,[+] Dr. H. Iida, Prof. E. Yashima
Department of Molecular Design and Engineering
Graduate School of Engineering, Nagoya University
Chikusa-ku, Nagoya 464-8603 (Japan)
E-mail: qisl@mail.buct.edu.cn
yashima@apchem.nagoya-u.ac.jp
Dr. L. Liu, Prof. S. Irle
Department of Chemistry, Graduate School of Science
Nagoya University, Chikusa-ku, Nagoya 464-8602 (Japan)
E-mail: sirle@iar.nagoya-u.ac.jp
Prof. W. Hu
Beijing National Laboratory for Molecular Sciences
Key Laboratory of Organic Solids, Institute of Chemistry
Chinese Academy of Science, Beijing 100190 (China)
[+] Present address: State Key Laboratory of Chemical Resource Engineering, Beijing University of Chemical Technology
Beijing 100029 (China)

[**] This work was supported by a Grant-in-Aid for Scientific Research (S) from the Japan Society for the Promotion of Science (JSPS), the Knowledge Cluster Initiative "Nagoya Nano-Technology Manufacturing Cluster," and the Global COE Program "Elucidation and Design of Materials and Molecular Functions" of the Ministry of Education, Culture, Sports, Science, and Technology (Japan). S.Q. thanks the JSPS for a postdoctoral fellowship for foreign researchers (P09252). L.L. thanks the Global COE Program for a doctoral fellowship. S.I. acknowledges support from the CMSI program, MEXT (Japan).

Supporting information for this article is available on the WWW under http://dx.doi.org/10.1002/anie.201208481.

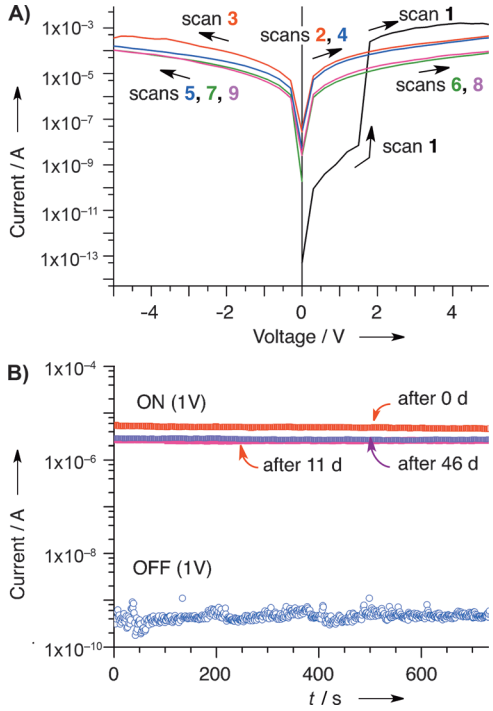

Figure 2. A) Current–Voltage characteristics of the sandwich device using the st-PMMA/C_{60} inclusion complex (20 wt% C_{60}) as the active layer. The sweep sequence and direction are indicated by the number and arrow, respectively (scans 1, 2, 4, 6, and 8: 0 to +5 V; scans 3, 5, 7, and 9: 0 to −5 V). B) Effect of operation time (at 1 V stress) on the device current at the ON and OFF states, tested under ambient conditions. The ON state device current was further traced intermittently for 46 days after the first switch.

Figure 2A shows the electrical switching effect of the C_{60} molecular wires demonstrated by the current-voltage (*I–V*) characteristics of an ITO/st-PMMA/C_{60}/Au sandwich device composed of an st-PMMA/C_{60} inclusion complex containing 20 wt% of C_{60}. During the first sweep from 0 to 5 V, an abrupt increase in the current density was observed at a threshold voltage of about 1.5 V, which indicates that the device switched from a low-conductivity (OFF) state to a high-conductivity (ON) state. The device remained in its high-conductivity state during the subsequent positive sweep (the 2nd scan), however, the subsequent negative scan from 0 to −5 V (the 3rd scan) did not turn the device from the ON state to the OFF state. Unfortunately, a reversible electrical switching effect was not observed, but the device essentially kept this high-conductivity state (although it gradually relaxed) during the following forward (scans 4, 6, and 8) and reverse sweeps (scans 5, 7, and 9), thus indicating the irreversible or "unerasable" characteristics of the electrical switching. Subsequent measurements showed that the device further remained in the ON state after turning off the power, thus revealing its nonvolatile features. The ON state current gradually decreased during the bias scanning process, but finally stabilized at a slightly lower level after the 6th scan (Figure 2A). As reported, memory devices with such electrical characteristics can serve as write-once-read-many-times (WORM) memory[11] in information storage. The switching-ON process corresponds to the writing process in digital memory. The distinct bistable electrical states in the voltage range of 0–1.5 V allows a voltage (1.0 V) to read the OFF or 0 signal (before writing) and ON or 1 signal (after writing) of the device. Further experiments using different st-PMMA/C_{60}-based sandwich devices revealed that the observed *I–V* characteristic was repeatable, but with variations in the switching voltage from 1.2 to 2.5 V and ON/OFF current ratio of 10^3–10^6. Hence, it is concluded that the st-PMMA/C_{60} inclusion complex could provide an irreversible electrical switching effect and can be used for WORM memory.

However, a pristine st-PMMA and st-PMMA/C_{60} inclusion complex containing 10 wt% C_{60} did not show any special electrical characteristics (Supporting Information, Figure S1 a,b), which implies that fullerene concentrations have a significant influence on the electrical switching effect. Moreover, the st-PMMA (*mm/mr/rr* = 1:5:94) isomers, atactic (at)-PMMA (*mm/mr/rr* = 9:39:52) and isotactic (it)-PMMA (*mm/mr/rr* = 94:3:3) were also employed for comparison. However, electrical switching was not observed with the sandwich devices using at-PMMA/C_{60} or it-PMMA/C_{60} as active layers, no matter how many C_{60} molecules (0, 10, or 20 wt%) were included (Figure S1 c–h). The distinct electrical behaviors observed between the st-PMMA/C_{60} and the at- or it-PMMA/C_{60} systems can be explained by differences in their encapsulation of fullerenes.

The st-PMMA chains have been demonstrated to fold into a helix of 74 units per 4 turns with a helical cavity of about 1 nm, which is self-tunable to encapsulate C_{60}, C_{70}, and C_{84} to yield the 1D fullerene arrays.[7a] However, the at- and it-PMMAs do not have this ability to produce 1D C_{60}-based molecular wires, as supported by their differential scanning calorimetry (DSC) and X-ray diffraction (XRD) measurement results (Figure S5–S9); their profiles were completely different from those of the st-PMMA/C_{60} films, in which the st-PMMA/C_{60} inclusion complex showed a crystalline structure (Figure S2–S4).[7a,12] Unlike the fullerenes in st-PMMA, fullerenes in the at- and it-PMMAs were not confined to the 1D peapod arrays, but were instead self-aggregated and randomly embedded in the matrix. The structural differences observed here suggest that the 1D C_{60}-based molecular wires formed in the polymer play an essential role in realizing the electrical switching effect.

For practical applications, the ON/OFF current ratio and device stability are always important for memory device performance. Figure 2B displays the ON and OFF current tested under ambient conditions. Under a constant bias of 1 V, no obvious change in the current density was observed for the OFF and ON states during short-term operation, and the device achieved an ON/OFF current ratio of more than 10^4. The device maintained its high-conductivity state after being switched ON, but gradually relaxed to a low conductance level after a long operation time, as can be seen in Figure 2B, where gradual current degradation occurred during the continuous bias sweep process. The ON/OFF ratio of the devices 11 days after the first measurement was reduced to around 7000. However, further investigation after 46 days revealed that the devices had stabilized at this conductive level and did not show any further degradation. This ON/OFF

current ratio in the present device would promise a low misreading rate during use in digital memory applications.

For a mechanistic understanding of the irreversible electrical switching effect and the current degradation behavior observed in the st-PMMA/C_{60} inclusion complex, quantum chemical calculations were performed on the C_{60} molecular wires during the charge injection process using a self-consistent-charge density-functional tight-binding method with a dispersion correction (SCC-DFTB-D).[13] The geometries of the linear, neutral C_{60} wires, consisting of 1–20 C_{60} molecules (Figure 3 A and Table S1) were first optimized.

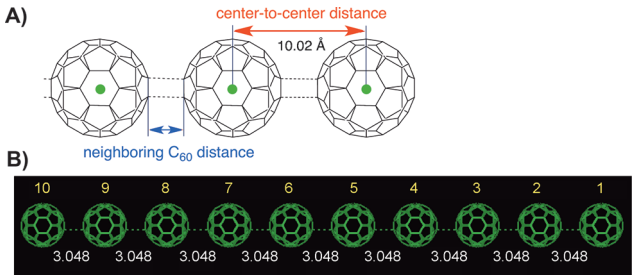

Figure 3. A) Illustration of the initial C_{60}-based molecular wire used in the SCC-DFTB-D simulation. B) The geometry of the C_{60}-based molecular wire with 10-C_{60} molecules after optimization.

After testing a wide range of different chain lengths, we finally selected a chain of 10 C_{60} molecules (10-C_{60}; Figure 3 B) as the model to represent the C_{60} wires. This was chosen because the electronic properties, especially the energy gaps for the wires, are converged with respect to the number of C_{60} units at this size (Figure S10). We noted that the computed band gap (ca. 1.63 eV) agrees well with the experimental value (1.7 eV),[1b] thus indicating the validity of the SCC-DFTB-D method in predicting the properties of the C_{60} wires.

Figure 4 shows the changes in the distances between the neighboring C_{60} molecules observed in the 4-C_{60} (A) and 10-C_{60} (B) molecular wires during the charge injection process. As observed in Figure 4, a violent Coulomb explosion[14] suddenly occurrs at a critical charge point (see the Supporting Information), resulting in the significant separation of the C_{60} molecules from each other in the C_{60} wires. We identify this Coulomb explosion as the event responsible for the irreversible electrical switching effect observed in the st-PMMA/C_{60} inclusion complex (see below for further discussion). The average charge on each C_{60} in the 4-C_{60} peapod-like molecular wire was 3.5 electrons ($14\,e^-/4 = 3.5\,e^-$) at the Coulomb explosion point (Figure 4 A), whereas they were reduced to 2.7 e^- ($27\,e^-/10 = 2.7\,e^-$) in the 10-C_{60} molecular wire (Figure 4 B), which indicates that the accumulated Coulomb explosion likely occurs relatively easily in long C_{60} molecular wires.

Figure 5 A shows the average energy changes (ΔE) per C_{60} molecule as a function of the average charge loaded on each C_{60} molecule in the C_{60} wires with a different number of C_{60} units. These data clearly indicate that the longer C_{60} molecular wires are higher in energy and hence become unstable,

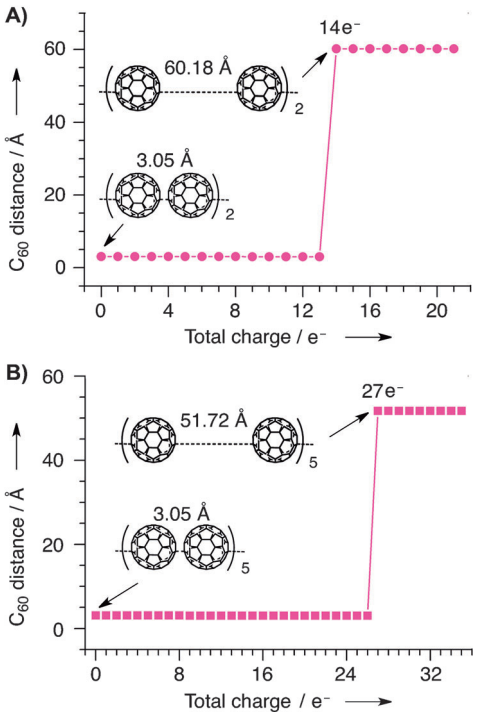

Figure 4. Changes in neighboring C_{60} distances with increasing charges on the 4-C_{60} (A) and 10-C_{60} (B) molecular wires (for details see Tables S2 and S3, respectively). Note that the large C_{60} distances are determined by the force thresholds applied in the employed conjugate gradient geometry optimization algorithm.

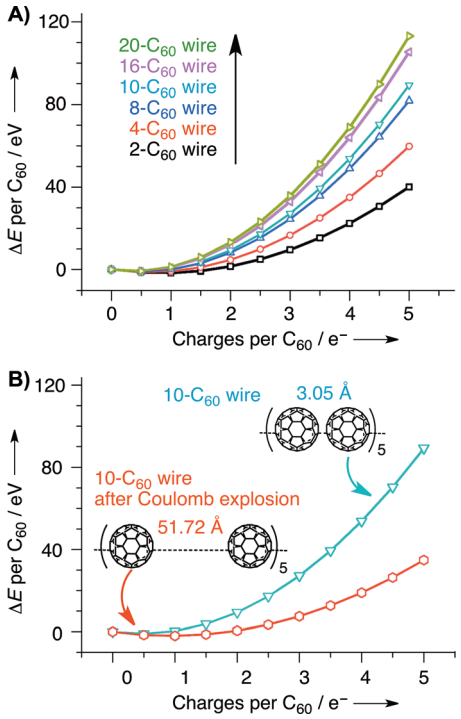

Figure 5. The average energy changes (ΔE) per C_{60} molecule as a function of the average charge loaded on each C_{60} molecule in the C_{60}-based molecular wires with different C_{60} numbers (A) and in the 10-C_{60} molecular wire before and after Coulomb explosion at 27 e^- (B). Only single-point energy calculation was done here; see Table S4 for more details.

accordingly they have a stronger thermodynamic tendency to break up into shorter wires, which is consistent with the results in Figure 4. This also means that charge injection into longer C_{60} wires is more difficult, as more energy is needed for loading the same charges. Figure 5B displays the same relationship for the 10-C_{60} molecular wire as in Figure 5A, but shows the relative energies before and after the Coulomb explosion at 27 e^- (see Figure 4B), which suggest that the C_{60} molecular wire with the larger inter-C_{60} distances (after Coulomb explosion) is more favorable for charge injection.

The distinctly low energy barrier between the metal electrodes and the LUMO of C_{60} (Figure 1C) suggests that electrons can be readily injected into individual C_{60} molecules under a low bias voltage. However, the above simulation results remind us that charge injection into C_{60} molecular wires is significantly restricted during the initial voltage scan, because the C_{60} molecules are closely packed to form 1D C_{60} arrays in the insulated st-PMMA helical tube; therefore, the injected electrons can easily migrate along the C_{60}-based molecular wire, but not across the C_{60} wires in the different st-PMMA chains. As a result, electron hopping (tunneling) between the neighboring C_{60} molecular wires (perpendicular to the axis of the C_{60} wire), which is responsible for the real electrical conductance of the device, is severely limited. Concomitantly, the electrons injected into the C_{60} molecular wires will induce a countering space–charge field in the polymer matrices, which will screen the applied external electric field, thereby inhibiting further charge injection into the active layer.[15] Thus, the material exhibits a high-resistance state, and the device shows only a limited increase in the current below 1.5 V.

Under further applied voltage over 1.5 V, negative charges are then injected into the C_{60} wires, which induces a highly energetic and unstable state, eventually leading to a violent Coulomb explosion, which separates the continuous and closely-aligned peapods into short wires or even isolated C_{60} molecules, both inside and outside the st-PMMA cavity. Consequently, during further voltage sweeps, charge loading into the C_{60} molecules will be greatly facilitated, as previously clarified. The significantly increased inter-C_{60} distances will greatly restrain the charge transport along the C_{60} molecular wires, which instead tolerates the inter-wire charge hopping between the C_{60} wires. Therefore, the percolation pathways for charge carriers among the C_{60} molecules will be generated, triggering the device to a high conductance state under applied external electric field. The lack of electrical switching in the st-PMMA/C_{60} inclusion complex containing 10 wt% C_{60} may be explained by its low C_{60} content, which results in the difficult formation of tightly-aligned C_{60} molecular wires. This speculation is supported by the fact that the st-PMMA helical hollow spaces would be filled with ca. 28 wt% C_{60} molecules.[7a] Hence, it seems reasonable to deduce that, after Coulomb explosion, the separated C_{60} molecules could not recover the initial closely-aligned C_{60} wires. Consequently, the device shows an irreversible switching behavior. Although partial re-formation of the C_{60} wires through local C_{60} recombination may theoretically be possible, their contribution to the device performance is likely small owing to the limited diffusion of C_{60} molecules inside st-PMMA solid thin films.

In summary, an irreversible electrical switching effect has been demonstrated in the st-PMMA/C_{60} inclusion complex loaded with 20 wt% C_{60} when used as the active layer in a sandwiched device. The device showed a final ON/OFF current ratio of around 7000, which allows this system to be used as nonvolatile write-once-read-many-times memory. The systematic investigations using PMMAs with different tacticities revealed that a supramolecular peapod-like molecular wire formation of C_{60} molecules within the st-PMMA helical cavity is indispensable for achieving the electrical switching behavior. Detailed quantum chemical calculations suggest that a violent Coulomb explosion occurs at the C_{60}-based molecular wire during the charge injection process, which accounts for the electrical features observed in the current work. Although the present device performance, including the ON/OFF current ratio, may not reach a satisfactory level for practical applications, the st-PMMA/C_{60} inclusion complex distinguishes itself from other nanomaterials by its unique 1D-ordered nanopeapod-like structure, high monodispersity, controlled morphology, structural reproducibility, large-scale synthetic capability, as well as its easy processability and scalability. These advantages will open the way for the further development of novel fullerene-based nanomaterials with practical applications in optoelectronics.

Received: October 22, 2012
Published online: December 13, 2012

Keywords: density functional tight-binding theory · electrical switching · fullerenes · nanotubes · poly(methyl methacrylate)

[1] a) T. Anthopoulos, F. Kooistra, H. Wondergem, D. Kronholm, J. Hummelen, D. de Leeuw, *Adv. Mater.* **2006**, *18*, 1679 – 1684; b) C. Sung, D. Kekuda, L. Chu, Y. Lee, F. Chen, M. Wu, C. Chu, *Adv. Mater.* **2009**, *21*, 4845 – 4849.

[2] a) Y. Wang, *Nature* **1992**, *356*, 585 – 587; b) B. Thompson, J. Frechet, *Angew. Chem.* **2008**, *120*, 62 – 82; *Angew. Chem. Int. Ed.* **2008**, *47*, 58 – 77; c) G. Dennler, M. Scharber, C. Brabec, *Adv. Mater.* **2009**, *21*, 1323 – 1338.

[3] a) J. Hou, J. Yang, H. Yang, Q. Li, C. Zeng, L. Yuan, B. Wang, D. Chen, Q. Zhu, *Nature* **2001**, *409*, 304 – 305; b) D. Guldi, F. Zerbetto, V. Georgakilas, M. Prato, *Acc. Chem. Res.* **2005**, *38*, 38 – 43; c) S. Babu, H. Mohwald, T. Nakanishi, *Chem. Soc. Rev.* **2010**, *39*, 4021 – 4035.

[4] a) B. Smith, M. Monthoux, D. Luzzi, *Nature* **1998**, *396*, 323 – 324; b) K. Hirahara, K. Suenaga, S. Bandow, H. Kato, T. Okazaki, H. Shinohara, S. Iijima, *Phys. Rev. Lett.* **2000**, *85*, 5384 – 5387; c) O. Vostrowsky, A. Hirsch, *Angew. Chem.* **2004**, *116*, 2380 – 2383; *Angew. Chem. Int. Ed.* **2004**, *43*, 2326 – 2329; d) A. Khlobystov, D. Britz, G. Briggs, *Acc. Chem. Res.* **2005**, *38*, 901 – 909; e) R. Kitaura, H. Shinohara, *Chem. Asian J.* **2006**, *1*, 646 – 655; f) L. Guan, K. Suenaga, S. Okubo, T. Okazaki, S. Iijima, *J. Am. Chem. Soc.* **2008**, *130*, 2162 – 2163.

[5] a) A. Rochefort, *Phys. Rev. B* **2003**, *67*, 115401; b) L. Ge, J. Jefferson, B. Montanari, N. Harrison, D. Pettifor, G. Briggs, *ACS Nano* **2009**, *3*, 1069 – 1076; c) A. Suzuki, T. Oku, K. Kikuchi, *Physica B* **2010**, *405*, 2418 – 2422.

[6] a) T. Kaneko, Y. Li, S. Nishigaki, R. Hatakeyama, *J. Am. Chem. Soc.* **2008**, *130*, 2714 – 2715; b) A. Eliasen, J. Paaske, K. Flens-

berg, S. Smerat, M. Leijnse, M. Wegewijs, H. Jorgensen, M. Monthioux, J. Nygard, *Phys. Rev. B* **2010**, *81*, 155431.
[7] a) T. Kawauchi, J. Kumaki, A. Kitaura, K. Okoshi, H. Kusanagi, K. Kobayashi, T. Sugai, H. Shinohara, E. Yashima, *Angew. Chem.* **2008**, *120*, 525 – 529; *Angew. Chem. Int. Ed.* **2008**, *47*, 515 – 519; b) T. Kawauchi, A. Kitaura, J. Kumaki, H. Kusanagi, E. Yashima, *J. Am. Chem. Soc.* **2008**, *130*, 11889 – 11891; c) T. Kawauchi, A. Kitaura, M. Kawauchi, T. Takeichi, J. Kumaki, H. Iida, E. Yashima, *J. Am. Chem. Soc.* **2010**, *132*, 12191 – 12193.
[8] a) H. Majumdar, J. Baral, R. Osterbacka, O. Ikkala, H. Stubb, *Org. Electron.* **2005**, *6*, 188 – 192; b) S. Paul, A. Kanwal, M. Chhowalla, *Nanotechnology* **2006**, *17*, 145 – 151; c) A. Kanwal, M. Chhowalla, *Appl. Phys. Lett.* **2006**, *89*, 203103; d) S. Cho, D. Lee, J. Jung, T. Kim, *Nanotechnology* **2009**, *20*, 345204.
[9] C. Reed, R. Bolskar, *Chem. Rev.* **2000**, *100*, 1075 – 1120.
[10] L. Bozano, B. Kean, M. Beinhoff, K. Carter, P. Rice, J. Scott, *Adv. Funct. Mater.* **2005**, *15*, 1933 – 1939.
[11] S. Möller, C. Perlov, W. Jackson, C. Taussig, S. Forrest, *Nature* **2003**, *426*, 166 – 169.
[12] The C_{60} precipitated upon evaporating the solvent from an it-PMMA/C_{60} mixture in toluene (Figure S9), and significant C_{60} aggregation was also confirmed by optical microscopic and atomic force microscopy (AFM) images of it-PMMA/C_{60} films. C_{60} is miscible with at-PMMA at low C_{60} concentrations ($\leq$ 10 wt%; Figure S5 and S6), but its mixture readily segregates at higher C_{60} content (20 wt%) upon solvent evaporation or thermal treatment of the at-PMMA/C_{60} mixture films at 100–160 °C, as evidenced by the appearance of sharp C_{60} reflection peaks in their XRD profiles (Figure S7 and S8).
[13] a) M. Elstner, D. Porezag, G. Jungnickel, J. Elsner, M. Haugk, T. Frauenheim, S. Suhai, G. Seifert, *Phys. Rev. B* **1998**, *58*, 7260 – 7268; b) M. Elstner, P. Hobza, T. Frauenheim, S. Suhai, E. Kaxiras, *J. Chem. Phys.* **2001**, *114*, 5149 – 5155; c) B. Aradi, B. Hourahine, T. Frauenheim, *J. Phys. Chem. A* **2007**, *111*, 5678 – 5684.
[14] G. Liu, Y. Zhao, K. Zheng, Z. Liu, W. Ma, Y. Ren, S. Xie, L. Sun, *Nano Lett.* **2009**, *9*, 239 – 244.
[15] G. Liu, Q. Ling, E. Kang, K. Neoh, D. Liaw, F. Chang, C. Zhu, D. Chan, *J. Appl. Phys.* **2007**, *102*, 024502.

